Trails of Kilovolt Ions Created by Subsurface Channeling

Alex Redinger,[1] Sebastian Standop,[1] Thomas Michely,[1] Yudi Rosandi,[2] and Herbert M. Urbassek[2,*]

[1]*II. Physikalisches Institut, Universität Köln, Zülpicherstraße 77, D-50937 Köln, Germany*

[2]*Fachbereich Physik und Forschungszentrum OPTIMAS, Universität Kaiserslautern, Erwin-Schrödinger-Straße, D-67663 Kaiserslautern, Germany*

(Received 18 September 2009; published 18 February 2010)

Using scanning tunneling microscopy, we observe the damage trails produced by keV noble-gas ions incident at glancing angles onto Pt(111). Surface vacancies and adatoms aligned along the ion trajectory constitute the ion trails. Atomistic simulations reveal that these straight trails are produced by nuclear (elastic) collisions with surface layer atoms during subsurface channeling of the projectiles. In a small energy window around 5 keV, Xe^+ ions create vacancy grooves that mark the ion trajectory with atomic precision. The asymmetry of the adatom production on the two sides of the projectile path is traced back to the asymmetry of the ion's subsurface channel.

DOI: 10.1103/PhysRevLett.104.075501 PACS numbers: 61.80.Jh, 68.37.Ef, 79.20.Ap, 79.20.Rf

The interaction of keV ion beams with surfaces has encountered renewed interest recently due to their ability to create regular dot and ripple patterns on the nanoscale [1–3]. These regular patterns have a significant potential for applications ranging from the modification of wetting and optical reflectivity, via patterned adsorption to data storage [4]. Evidently, the understanding of pattern formation requires a detailed, atomistic knowledge of single ion-surface interaction, and, in particular, of damage formation and healing.

Upon grazing incidence, highly regular ripple patterns with ridges aligned with the ion beam direction evolve on metals [5,6], oxides [7], and alkali halides [8]. It was soon realized that for the formation and regularity of these patterns subsurface channeling should be of decisive importance [6,8]. In subsurface channeling the ion enters the crystal under a small angle with respect to a low index surface (and often a low index direction)—typically at an ascending step—and then moves immediately below the surface layer [9,10]. Like in bulk channeling [11–13], the ion is then steered by atomic rows (or planes) along its path, thereby preventing close encounters with atoms. The ion energy loss per unit length is greatly diminished and its range extended.

Here we show experiments that visualize for the first time the trajectory of an ion performing subsurface channeling. The channeling particle leaves behind a trail of adatoms and surface vacancies which mark the ion trajectory with atomic precision. Guided by the molecular dynamics (MD) simulations accompanying our experiments we are even able to create a new type of nanostructure on Pt(111) for Xe^+ ions of appropriate energy: one- or two-atom-wide continuous rows of vacancies, $\approx$50 nm long and aligned along a high symmetry direction.

The ion trails of keV ions formed by nuclear (elastic) energy loss are reminiscent of the ion tracks of swift heavy MeV ions which result from electronic (inelastic) energy loss [14]. However, instead of keV/Å for swift heavy ions, only eV/Å are dissipated in the target by the channeling keV ions. It has to be noted that previously surface images of the impact points of ions with keV kinetic or potential energy were obtained [15–17], but not of extended ion trajectories.

Details of the interaction of grazing incidence ions with surfaces such as the asymmetry of damage production, the dependence of the ion trails on ion species, energy and angle of incidence, the phenomena of cross channeling, and the onset of subsurface channeling are now accessible through direct experiments and can be analyzed with the help of MD simulations as discussed here. We believe that our findings are thus not only of fundamental interest but also constitute a significant step towards a quantitative understanding of pattern formation under grazing incidence ion bombardment.

A clean Pt(111) surface was prepared according to standard procedures [6] in a variable temperature STM system with base pressure $<5 \times 10^{-11}$ mbar. At a grazing angle ϑ with respect to the surface normal ions are reflected off the perfect surface (surface channeled) and leave no or only negligible damage behind [6]. Therefore, we created large hexagonal vacancy islands bounded by monatomic steps prior to the single impact experiments [15]. The temperature T for the subsequent single impact experiments (fluence 1.5×10^{16} ions/m^2, $\vartheta = 86°$ or 78.5°, incidence along the $[1\bar{1}0]$ azimuth) was as low as possible to prevent diffusion of defects created—thereby enabling comparison to MD simulations—but high enough to prevent adsorption of the ions. For Ar^+ (Xe^+) we set $T = 62$ K ($T = 115$ K) during ion exposure and quenched subsequently to 20 K (105 K) for STM imaging. At 62 K only interstitials, at 115 K additionally single adatoms are mobile. Thus, after Xe^+ exposure the adatom features imaged are dimers or

larger clusters. It has to be noted that due to the convolution with the finite STM tip size the images of adatoms and adatom clusters are exaggerated in extension. For the same reason surface vacancies or small clusters are typically invisible to the STM tip, especially if near adatom clusters. Also lines of vacancies appear just as slight depressions with a width of ≈ 0.1 Å in the surface.

Our MD simulations are performed in a standard way [18,19]. The target crystallite has a size of 298 Å along the ion direction, and is 86 Å broad, consisting of 18 Pt(111) layers. The topmost layer ends at 120 Å to form an ascending step. In total, a number of 625 ion trajectories were simulated, which varied in the location of the ion impact point with respect to the step edge. The Pt interatomic interaction is described by a many-body interaction potential [20] which is splined at high energies to the ZBL repulsive potential [21]. The interaction between the noble-gas ions and the target atoms is modeled to be purely repulsive according to the ZBL potential. All simulations are performed at 0 K; at higher temperatures the length of the trajectories, but not the damage patterns, are changed [22]. For the defect analysis, we follow the atom trajectories up to 25 ps.

The STM topograph of Fig. 1(a) displays characteristic impact patterns of 5 keV Xe^+. An ion may hit step atoms and induce a thermal spike resulting in a crater surrounded by an adatom rim as in event (1). However, frequently a Xe^+ creates a continuous vacancy groove of one- or two-atom width with adatoms nearby as in event (2). For about 15% of all impacts the vacancy groove extends over more than 200 Å as for event (3). For Ar^+, Fig. 1(b), a similar diversity of impact patterns is found, but continuous vacancy grooves are never observed. The ion trail is formed by aligned adatoms as in event (4), while the created vacancy clusters are mostly invisible to STM. Ar^+ trails may be considerably longer than Xe^+ trails.

The MD simulations exemplified by Figs. 1(c)–1(f) show that the key process for the formation of the trail patterns as in events (2) to (4) is subsurface channeling of the ion underneath the first (or sometimes second) layer of atoms. The ion trajectory uses a surface step to enter a channel parallel to the surface plane and performs an oscillatory motion in the channel around its axis.

Figure 1(f) demonstrates that the Ar^+ creates adatoms whenever it hits the surface layer from below. In a similar, but less obvious, manner Xe^+ sputters atoms primarily when the ion is close to the surface layer, Fig. 1(d); however, this ion removes atoms continuously from the surface layer. Note also that the oscillation amplitude of the Xe^+ trajectory is significantly reduced compared to that of Ar^+. While the smaller Ar^+ fits in the Pt surface channel at the energy of 5 keV, the bigger Xe^+ permanently gives energy to the surface atoms and hence produces a continuous groove. According to our simulations presented in Fig. 2, the (elastic) stopping force, i.e., the average energy loss per unit length dE/dx, of a well-channeled Xe^+ exceeds that of an Ar^+ by almost 1 order of magnitude. Therefore, in addition to adatom production as for Ar^+, channeled Xe^+ ions cause a huge amount of sputtering.

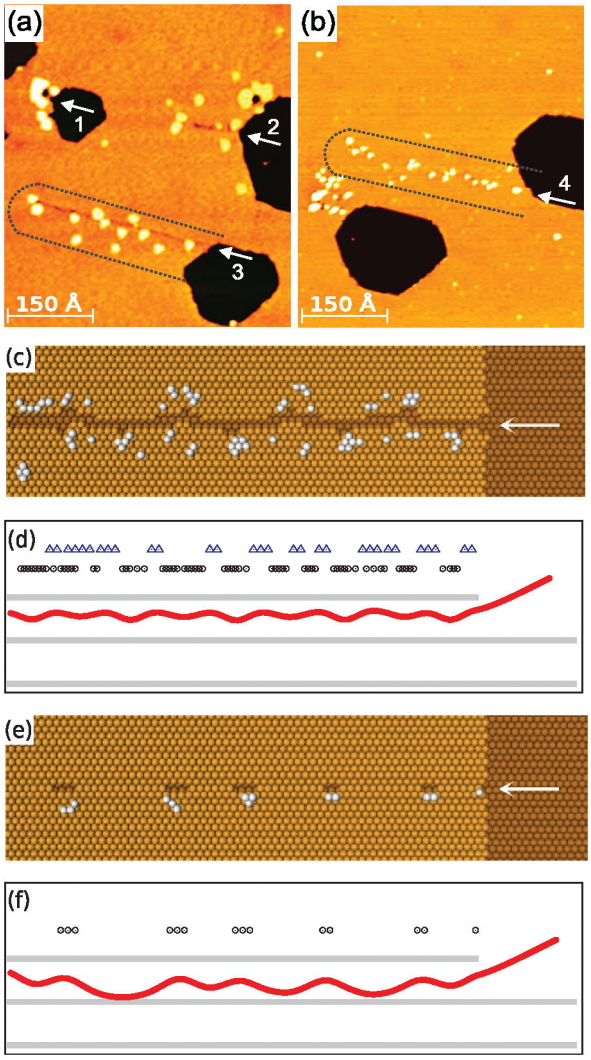

FIG. 1 (color). STM topographs after exposure with 5 keV Xe^+ (a) or Ar^+ (b) ions incident at $\vartheta = 86°$. Ion direction indicated by arrows. Dashed lines delineate damage regions of single ions. The image sizes are 580 Å × 490 Å. Top and side views of damage production for 5 keV Xe^+ (c),(d) and Ar^+ (e), (f) impacts, as simulated by MD [25]. In (d),(f) simulated trajectories are shown in red. Gray horizontal lines denote the atomic (111) planes, including the step edge. Black circles (blue triangles) above the (111) surface plane denote the locations from which adatoms (sputtered atoms) originate.

While bulk channeling is characterized by no or little damage formation before the ion dechannels, subsurface channeling, by contrast, makes itself felt by continuous or regularly spaced damage on the surface. This apparent contradiction is explained by the size of the energy barriers which have to be overcome to produce permanent damage: While in the bulk atoms need to be displaced with considerable energy through the surrounding cage of nearest neighbors to escape from their original site, surface atoms

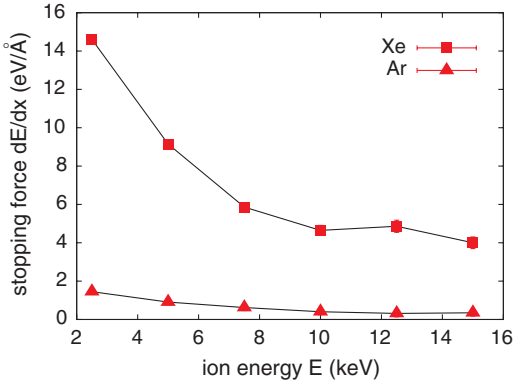

FIG. 2 (color online). Stopping force of Xe^+ and Ar^+ ions moving with energy E in a $[1\bar{1}0]$ channel deep inside the simulation cell. Data taken as an average over an ensemble of 500 ions which were well channeled over a length of at least 80 Å. Error bars are smaller than the symbol size.

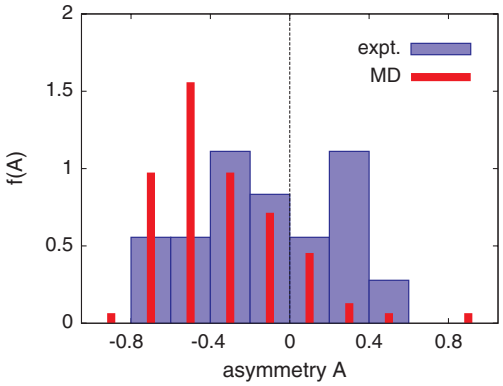

FIG. 3 (color online). Experimental (blue) and simulation (red) results for the distribution $f(A)$ of the adatom asymmetry A, Eq. (1), for 5 keV Xe^+ ions incident at $\vartheta = 86°$ channeling along the $[1\bar{1}0]$ direction.

are pushed with little effort onto the surface. For Pt, the bulk displacement energy is 34 eV [23], whereas the surface displacement energy amounts to only 2.3 eV [24].

The simulation data of the stopping force of channeled ions (Fig. 2) show a clear dependence on ion species and energy, which explains why surface-vacancy groove formation is observed only in a narrow energy window. The data have been taken for Xe^+ ions moving in the $[1\bar{1}0]$ channel along the channel axis by measuring their average elastic energy loss per unit length; we verified that a small tilt towards the channel axis, such as when the projectile is inserted via a surface step into the channel, has negligible influence on the energy loss. Note that only the elastic (nuclear) energy loss has been included here; we assume that inelastic (electronic) energy loss will shorten the ion trajectory, but not influence the damage production process. Stopping substantially decreases with ion energy up to ion energies of around 10 keV. This decrease is due to an increase in the channel width with ion energy, cf. Fig. 4 below; this increases the wavelength of channeled ions in the channel and reduces the number of ion-wall collisions. Indeed, our experiments show that for Xe energies beyond 10 keV no continuous vacancy grooves are formed in the initial, high energy parts of the trails.

Simulation shows that the length of the channeled trajectory depends on the exact entry position of the ion at the step edge and on thermal fluctuations of the lattice. During channeling, the ion may switch to a neighboring channel of the same orientation ["cross channeling"; see Fig. 1(c)]; when it eventually dechannels by a violent collision with a target atom, a larger amount of damage is created on the surface. For 5 keV, channeled trajectories with lengths of up to 400 Å (Xe) and 1000 Å (Ar) are observed in the experiments.

Event 3 in Fig. 1(a) demonstrates that the number of adatoms produced to the left of the ion trajectory, A_{left}, strongly exceeds that produced to the right, A_{right}. A strong adatom production asymmetry is also observed in the MD simulation events shown in Figs. 1(c) and 1(e). We present in Fig. 3 the distribution $f(A)$ of the asymmetry A defined as

$$A = \frac{A_{\text{right}} - A_{\text{left}}}{A_{\text{right}} + A_{\text{left}}}. \tag{1}$$

Since, in experiment, only the events with a continuous vacancy groove allow an unambiguous determination of "left" and "right" defect production, the asymmetry is evaluated for Xe^+ only. For the experimental distribution we refer to the number of adatom clusters, as the exact number of atoms in a cluster cannot be resolved. The experimental average is $\bar{A} = -0.15$ and simulation gives $\bar{A} = -0.36$. In both cases, left-sided adatom production is clearly preferred; the deviations between the distributions may be partly due to the different counting strategies, and to the finite temperatures in experiment. A similar asymmetry is also found for other ϑ in the subsurface channeling regime.

To uncover the origin of the asymmetry we calculated the shape of the channel for the moving Xe^+ using the

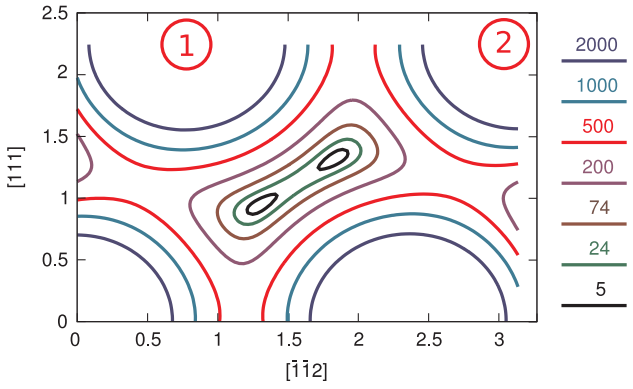

FIG. 4 (color). Equipotential lines (numbers in eV) for a 5 keV Xe^+ ion in a $[1\bar{1}0]$ channel calculated within the continuum approximation. The numbers 1 and 2 indicate the locations of the surface atoms bounding the subsurface channel.

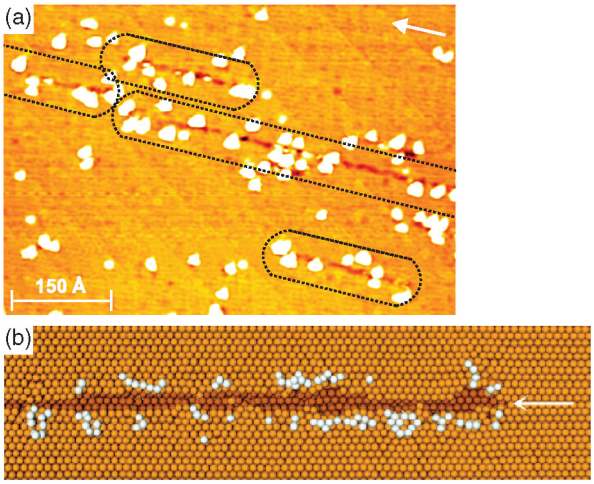

FIG. 5 (color). Vacancy groove formation by 5 keV Xe^+ ions incident with $\vartheta = 78.5°$ on a flat terrace. (a) STM topograph after low fluence ion exposure. The image size is 460 Å × 670 Å. Ion beam direction indicated by the arrow. (b) MD simulation damage pattern (top view) [25].

continuum approximation of the ZBL potential for the Xe-Pt interaction, Fig. 4. The three low-energy potential contour lines from 24 eV to 200 eV define the shape of the channel. For a 5 keV Xe^+ ion moving with 4° towards the channel axis, as in Fig. 1, the energy perpendicular to the channel axis, $E_\perp$, amounts to only 24 eV. The corresponding contour line is very narrow and asymmetric. For even smaller $E_\perp$ the channel splits into two subchannels. In our simulations we find that during their motion through the channel the ions are frequently confined to just one subchannel. Xe^+ ions moving in the upper subchannel transfer momenta to both Pt surface atoms labeled 1 and 2 in Fig. 4 and hence create adatoms symmetrically, $\bar{A} \cong 0$. However, Xe^+ ions moving in the lower subchannel can give momentum only to surface atom 1, hence $A < 0$. Thus, while the Xe^+ ion oscillates in its channel, the adatom production is predominantly left sided. Figure 1(d) exemplifies the motion of an ion caught in the upper subchannel, whereas the ion in Fig. 1(f) oscillates between both subchannels.

While at grazing angles ions are specularly reflected off a flat terrace, the situation changes at more oblique impact angles. If the kinetic energy of motion normal to the surface exceeds the height of the potential saddle point between surface atoms 1 and 2 in Fig. 4, ions may penetrate the flat terrace and enter a subsurface channel. Figure 5 displays experimental and simulated examples of 5 keV Xe^+ incident at $\vartheta = 78.5°$ entering a subsurface channel under a flat terrace. We observed these events for $\vartheta < 80°$. At 78.5°, we estimate from our simulations that 24% of the ions penetrate the crystal surface and create a vacancy groove during subsequent subsurface channeling.

This work has been supported by the Deutsche Forschungsgemeinschaft through project *Atomic scale surface damage by ion bombardment at grazing incidence*.

*urbassek@rhrk.uni-kl.de
URL: http://www.physik.uni-kl.de/urbassek/

[1] S. Facsko, T. Dekorsy, C. Koerdt, C. Trappe, H. Kurz, A. Vogt, and H. L. Hartnagel, Science **285**, 1551 (1999).
[2] B. Ziberi, F. Frost, T. Höche, and B. Rauschenbach, Phys. Rev. B **72**, 235310 (2005).
[3] W. L. Chan and E. Chason, J. Appl. Phys. **101**, 121301 (2007).
[4] An overview is given in a recent topical review, see R. Cuerno, L. Vázquez, R. Gago, and M. Castro, J. Phys. Condens. Matter **21**, 220301 (2009).
[5] S. van Dijken, D. de Bruin, and B. Poelsema, Phys. Rev. Lett. **86**, 4608 (2001).
[6] A. Redinger, H. Hansen, U. Linke, Y. Rosandi, H. M. Urbassek, and T. Michely, Phys. Rev. Lett. **96**, 106103 (2006).
[7] T. Luttrell, W.-K. Li, X.-Q. Gong, and M. Batzill, Phys. Rev. Lett. **102**, 166103 (2009).
[8] F. Krok, S. R. Saeed, Z. Postawa, and M. Szymonski, Phys. Rev. B **79**, 235432 (2009).
[9] K. Kimura, M. Hasegawa, and M. Mannami, Phys. Rev. B **36**, 7 (1987).
[10] C. Lemell, J. Stöckl, J. Burgdörfer, G. Betz, H. P. Winter, and F. Aumayr, Phys. Rev. Lett. **81**, 1965 (1998).
[11] G. R. Piercy, F. Brown, J. A. Davies, and M. McCargo, Phys. Rev. Lett. **10**, 399 (1963).
[12] M. T. Robinson and O. S. Oen, Phys. Rev. **132**, 2385 (1963).
[13] J. Lindhard, K. Dan. Vidensk. Selsk. Mat. Fys. Medd. **34**, No.14 (1965).
[14] R. L. Fleischer, P. B. Price, and R. M. Walker, *Nuclear Tracks in Solids* (University of California, Berkeley, 1975).
[15] T. Michely and C. Teichert, Phys. Rev. B **50**, 11 156 (1994).
[16] J. C. Kim, D. G. Cahill, and R. S. Averback, Surf. Sci. **574**, 175 (2005).
[17] A. S. El-Said *et al.*, Phys. Rev. Lett. **100**, 237601 (2008).
[18] A. Friedrich and H. M. Urbassek, Surf. Sci. **547**, 315 (2003).
[19] H. Hansen, C. Polop, T. Michely, A. Friedrich, and H. M. Urbassek, Phys. Rev. Lett. **92**, 246106 (2004).
[20] H. Gades and H. M. Urbassek, Nucl. Instrum. Methods Phys. Res., Sect. B **88**, 218 (1994).
[21] J. F. Ziegler, J. P. Biersack, and U. Littmark, *The Stopping and Range of Ions in Solids* (Pergamon, New York, 1985).
[22] A. Redinger, Y. Rosandi, H. M. Urbassek, and T. Michely, Phys. Rev. B **77**, 195436 (2008).
[23] R. S. Averback and T. Diaz de la Rubia, in *Solid State Physics*, edited by H. Ehrenreich and F. Spaepen (Academic Press, Boston, 1998), Vol. 51, p. 281.
[24] H. Gades and H. M. Urbassek, Phys. Rev. B **50**, 11 167 (1994).
[25] See supplementary material at http://link.aps.org/supplemental/10.1103/PhysRevLett.104.075501 for computer animated videos of the processes.